

Field Measurements in the BaBar Solenoid

Evgeny Antokhin, Adam Boyarski, Fatin Bulos, Alexey Buzykaev, William Dunwoodie, Sergey Ganzhur, Dave Jensen, Lewis Keller, Harvey Lynch, Nancy Yu, and Zachary Wolf

Abstract

The magnetic field within the BaBar super conducting solenoid (3.8m long by 3m diameter, at a field of 1.5 Tesla) has been measured with a set of hall probes placed on a mechanical arm that rotated about, and moved along, the axis of the coil. The measurements were fit to a functional model which contains polynomial terms to order 40 for the B_Z and B_R field components, a few trigonometric-bessel terms having one-, two-, and six-fold ϕ symmetry, and 24 dipole terms positioned on the end plates to describe the non-uniform iron distribution of these plates. The measurements and the model agree to 1.7 gauss (rms) within the drift chamber tracking volume, and to 5 gauss in the fully mapped volume ($-1.8 \leq Z \leq 1.8\text{m}$, $R < 1.3\text{m}$).

Overview

The BaBar detector contains tracking and particle identifying devices that measure properties of tracks produced in the interaction region of the e^+ and e^- beams at PEP II. Two subsystems in the detector, the drift chamber and the silicon vertex chamber, provide the positions and angles of the charged particles. These chambers are also immersed in a 1.5 Tesla magnetic field so that the momentum of charged particles can be measured. The magnetic field is generated by a super conducting solenoid, 3.8m long and 3.0m in diameter. The coil is surrounded by an iron return path that has a hexagonal cross section, and by end plates (doors) that provide the pole faces for the field. An elevation view of the detector is shown in Figure 1. The doors can be moved out of the way for access to the chambers inside. The doors and the hexagonal sides are called the instrumented flux return (IFR) because they are constructed from multiple parallel plates of iron separated by spacers to provide gaps for tracking detectors that measure the trajectory and range of particles passing through the iron.

The magnetic field within the tracking volume of the drift chamber ($R < 0.8\text{m}$, $|Z| < 1.4\text{m}$, and particle production angles between 17 to 255 degrees) must be known to high precision. The field outside of the tracking volume need not be known that precisely since the particle trajectories in this region are smeared by multiple scattering in the DIRC and calorimeter systems.

This document deals with the magnetic field produced by the solenoid in the absence of any PEP II beam line components, namely the B1 and Q1 permanent magnets located on the axis within the solenoid. These permanent magnets produce fringe fields of approximately 100-200 gauss at the inner layers of the drift chamber[1].

Note that the Z-coordinate system used in this document is zero at the center of the magnet. The interaction point is at -370mm in this coordinate system.

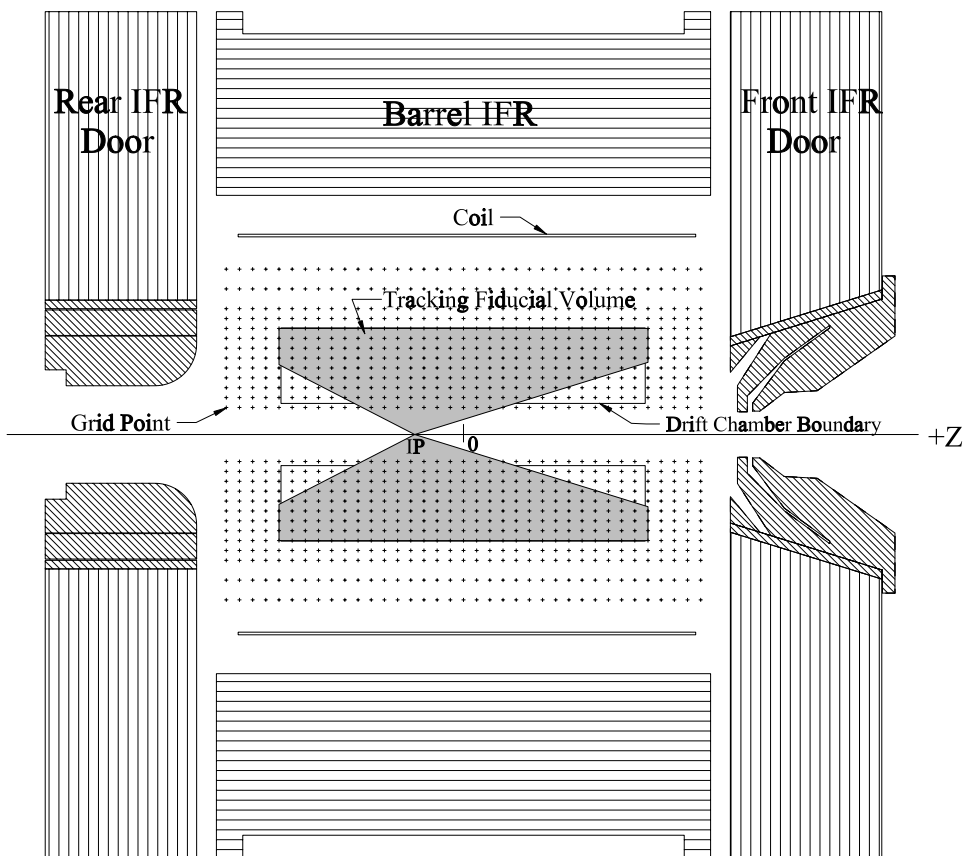


Figure 1. An elevation view of the BaBar magnetic solenoid is shown. The coil is enclosed by the instrumented flux return (IFR) iron in the barrel and doors. The magnetic field must be known with high precision within the tracking fiducial volume shown in the shaded region. The field measurements were made at the grid points marked with plus signs.

The question arises as to how well the magnetic field must be known through out the tracking volume. The momentum resolution of the 40-layer drift chamber is at best approximately 0.3% if the field is known perfectly. This implies that the random errors in the field determination need not be better than about a tenth of a percent (15 gauss). However, systematic errors in the field determination can lead to momentum errors larger than the statistical error. Simulation studies[2] show that systematic field errors of only one or two gauss can produce visible changes in the parameters of reconstructed tracks, indicating that the field should be measured to better than 2 gauss within the tracking volume.

Another source of error in the field comes from the non-uniform distribution of iron in the end plates. Each end plate has a centrally located hole for placement of the PEP II beam line components. The rear end plate also has through holes for signal cables from the drift chamber and vertex chamber, holes for the plug removal assembly (rails and screw leads), and slotted holes for the DIRC bar boxes. Iron has also been removed in the top portion of the rear end plate to provide a channel for cryogenic services to the super conducting coil. All these holes reduce the longitudinal field and increase the transverse fields in the vicinity of the

holes. Finally, the IFR spacers add iron, thereby increasing the longitudinal field near the vicinity of these spacers. These features are illustrated in Figure 2 for the rear end plate and Figure 3 for the front end plates.

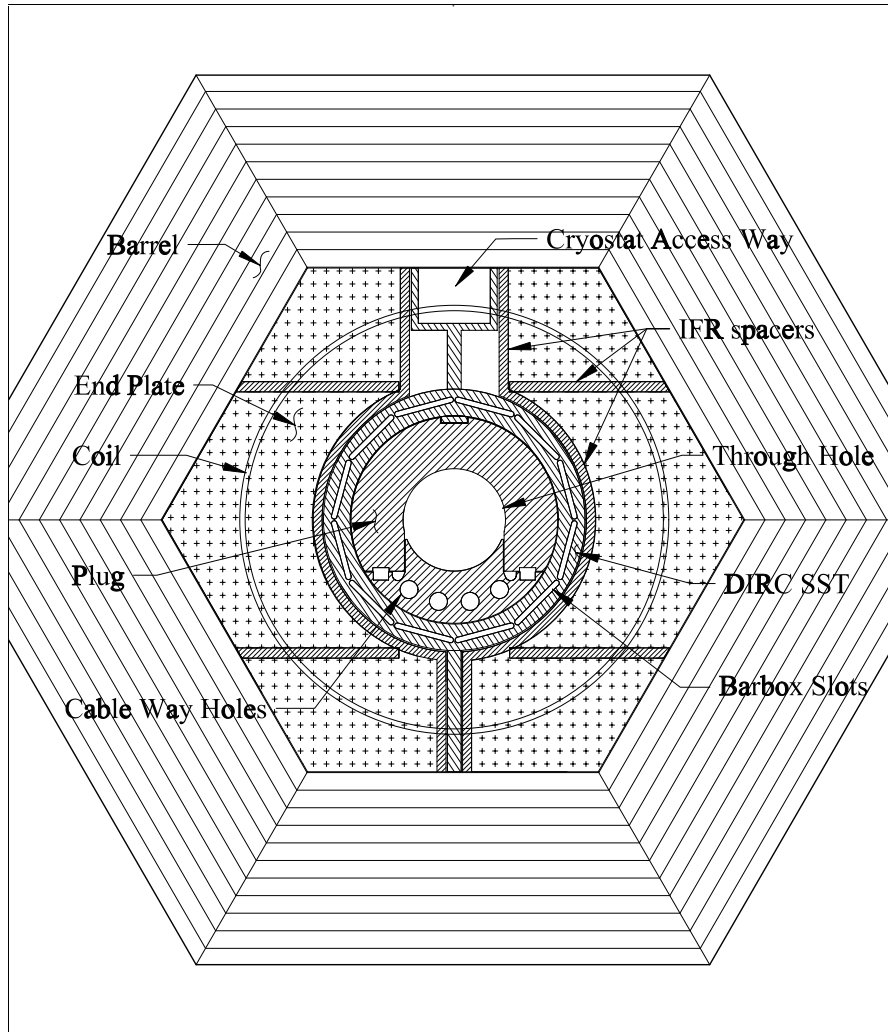


Figure 2 shows the magnetic material at the rear pole face comprising the rear door plate, the DIRC components, and the plug. The IFR spacers shown hold apart the lamination plates in the door. The DIRC components consist of the strong support tube with slots for the bar boxes, the top and bottom supports and a recess at the top for the access way to the cryostat. The plug has a central hole for beam line components and through holes for the cables ways and the plug rails and lead screws. The hexagonal shaped iron around the solenoid coil provides the flux return path.

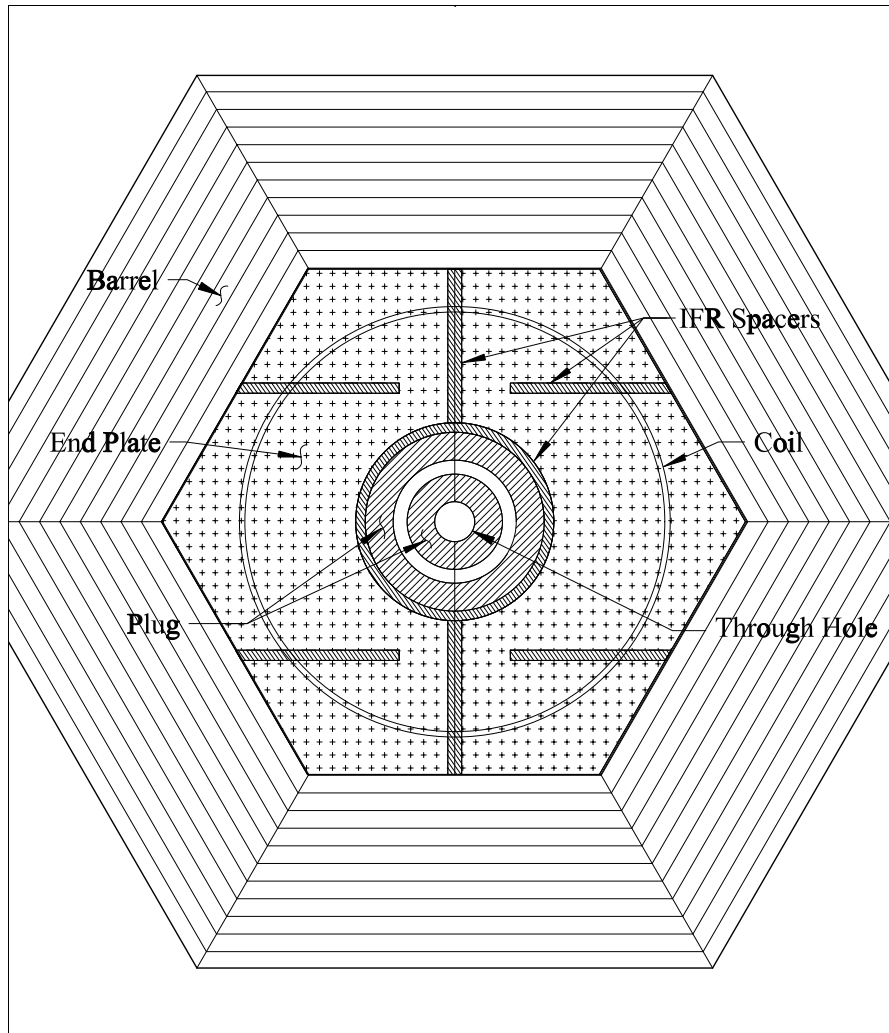


Figure 3. Magnetic material at the front pole face is similar to that for the rear, except that the plug is not removable, the central hole is smaller, and there are no other through holes.

The Measuring Apparatus

The magnetic field was measured by means of a transport mechanism that could move a set of Hall probes throughout the inside volume of the solenoid. Five probes were oriented in the Z direction, five in the radial (R) direction, and two in the phi direction to measure the B_Z , B_R , and B_ϕ field components respectively. These probes were equally spaced along a radial direction, each having the same phi. In addition, there was one NMR probe at a fixed R and a phi value 180° from that of the other probes that measured the total field near the central axis of the magnet.

The transport mechanism consisted of a long spindle with a rotating inner shaft held inside a pipe, with one end of the pipe rigidly attached to a cart on wheels. The cart moved on

precision rails along the spindle axis such that the spindle could travel through the central hole of the front end plate. This allowed the tip of the spindle to be positioned anywhere along the axis inside the solenoid with the end plate doors closed. A narrow plate (propeller) mounted at right angles to the rotating shaft at the tip end provided a platform for the probes. The probes were mounted rigidly on a separate plate, and this probe plate was in turn mounted on the propeller plate. In this way, the Z coordinate of the probes was controlled by the cart position on the rails, the phi coordinate by the rotation of the spindle shaft, and the R coordinate by the placement of the probe plate along the propeller arm. The Z and phi placement was done under computer control. The probe plate could be manually installed to one of three radial positions. The radial placement of the probe plate and the nominal coordinates of each probe on the plate are shown in Figure 4.

R (m)	Position 1	Position 2	Position 3
0.089	NMR	NMR	NMR
0.130	Bz1, Br1		
0.205		Bz1, Br1	
0.280	Bz2, Br2		
0.355		Bz2, Br2	
0.430	Bz3, Br3		
0.505	Bp1	Bz3, Br3	
0.580	Bz4, Br4	Bp1	
0.655	Bp2	Bz4, Br4	Bz1, Br1
0.730	Bz5, Br5	Bp2	
0.805		Bz5, Br5	Bz2, Br2
0.880			
0.955			Bz3, Br3
1.030			Bp1
1.105			Bz4, Br4
1.180			Bp2
1.255			Bz5, Br5

Figure 4 shows the nominal radial coordinates of the B_z , B_R , and B_ϕ Hall probes at each of three positions of the probe plate. All the probes are positioned along a radial line, so the phi coordinates are all the same. The NMR probe is fixed to the spindle (180° away from the other probes), so its R-coordinate does not change with plate position.

Each pair of high accuracy B_z and B_R probes[3] were encapsulated together in one unit, while the less accurate B_ϕ probe was an individual unit. The units had the shape of a square bar with a 14x14mm cross section, and the field sensitive point was at the cross section center, 9mm from one end of the bar. Signal cables came through the other end of the bar. These cables and the NMR signal cable were threaded through the spindle tube all the way to the cart and then to the digitizing electronics.

Predictions of the fields in the BaBar magnet were made using the MERMAID computer program. Comparisons of the measurements with the predictions gave comforting assurance that there were no gross errors in the measurements.

Data Sets

At each plate position, the shaft and probe arm were moved in a sequence of steps to provide measurements over a grid of points in Z and in phi. The Z grid ranged from -1.8m to +1.8m in steps of 0.1m, and phi ranged from 0° to 345° in steps of 15°. Some of the earlier data was taken with steps of 0.2m in Z for $|Z| < 1$ m. A data set consisted of a full sweep over the Z grid points, and a full sweep of the 24 phi-grid points at each Z setting. At each Z-phi grid point, the field readings from the 13 probes (5-Bz, 5-Br, 2-Bphi, and 1-NMR) were recorded, together with the coil current and environmental temperatures.

The following table shows the data sets that were taken at nominal field settings of 1.5T and 1.0T. Data set names ending with “a” are repeated cases, and sets ending with an “L” are measurements at the lower magnetic field.

Data Set	Plate Position	Field
1	1	1.5
2	2	1.5
2a	2	1.5
3	3	1.5
3a	3	1.5
2L	2	1
3L	3	1

The measurements were recorded in run files, with typically a few Z settings per run. Appendix A gives a list of the run numbers in chronological order for all the data sets.

Measurements were made at a standard reference point at $Z=0$ and $\phi=0$ between grid movements in Z. This provided a quality check for the measurements. Two probes (B_{Z3} , B_{Z4}) were found to have started drifting during the course of the measurements. These probes were dropped from the fits in data sets that showed any drifting, as shown in the last column in Appendix A.

Corrections to the Data

Knowing the placement and the alignment of the probes is crucial for measuring the magnetic field. For example, a 1-mrad rotation of a B_R probe in the R-Z plane results in an error of 15 gauss in that probe from the 15,000 gauss B_Z field. Corrections for the probe locations and the probe orientations were obtained from alignment measurements where possible, or from fits to the data when measurements were not possible.

Corrections from Surveyed Measurements

The SLAC alignment group positioned the axis of the mapping hardware on the axis of the detector. The plane of the propeller was also adjusted (by means of two turnbuckles on the top of the spindle tube near the tip end of the spindle) to be vertical to compensate for any droop from horizontal of the long spindle. However, as the spindle was moved in Z, small deviations of the center of rotation of the propeller and of the tilt of the probe plate were observed. Alignment surveys of the probe plate were made every time the probe plate was moved.

Two tooling balls placed along the radial length of the probe plate provided the tilt of the plate in the R-Z plane (giving mostly a B_R probe correction from the B_Z field, but also a B_Z probe correction where the B_R field was large). Two other tooling balls placed across the width of the plate measured the rotation of the plate in the plane perpendicular to R (giving mostly a B_ϕ probe correction from the B_Z field).

These alignment corrections were applied both to the probe coordinates as well as the probe field measurements. The latter required the knowledge of the three field components at a grid point. If one of the field components was not available at that grid point (due to a bad probe, or the phi probes being interspersed between the Z- and R-probes), then interpolation from other grid points was made. Later, as the fitting model improved, the missing field components were obtained from the fitting equations in an iterative fashion.

The following alignment measurements were made.

1. The X and Y coordinates of the center of rotation of the spindle tip were surveyed as a function of Z.
2. The deviations of the propeller's rotational axis (angles) from the detector axis in the horizontal and vertical planes were measured as a function of Z.
3. The probe plate angles were measured at phi steps of 45° between 0° to 315° degrees, and the plate angles at each of the phi grid point were found by interpolation from these.
4. The radial placement of the plate on the arm, and the relative Z and R locations of the probes on the probe plate were measured.

All of the above measurements, and a few parameters from the fit (next section), were used to correct and transform the probe coordinates, the probe angles, and the probe fields to the exact grid points.

Corrections by Fitting

The orientation of the field sensitive volume in the Hall probes must be known to better than 0.1mrad if the fields are to be measured to ≤ 2 gauss. Errors in the orientation come from the placement of the field sensitive volume within the probe, the positioning of the probe in its fixture, the fixture location on the plate, and the plate geometry (flexure). During the initial installation of the probes on the probe plate, the plate was put into a large dipole test magnet and the probe orientations were adjusted to null the B_R and B_ϕ signals. Even so, the correction angle of each B_R and B_ϕ probe was put as a parameter into the fit, with a set of such parameters for each data set (since the plate was moved between data sets). Figure 5 shows the probe orientations from the fit. There is a steady progression of the angle from -1.0 mrad to 0.5mrad with the probe number (i.e. R) for most data sets, implying that the plate is curved along the R direction.

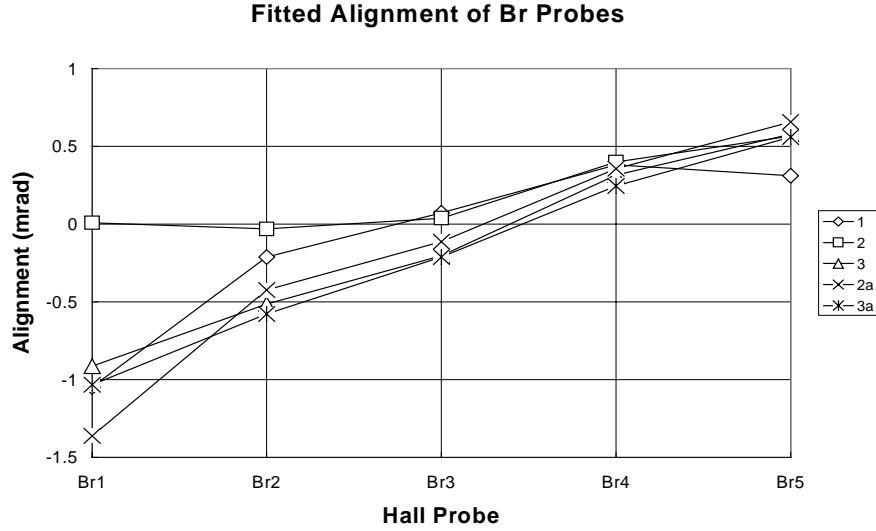


Figure 5. This plot shows the alignment obtained from the fit of the Br probes relative to the Z and R-axis. Separate alignment parameters were fit for each data set (1, 2, 3, 2a, and 3a). There is a general linear trend in the alignment error with the probe number, due to a curvature in the probe plate along the radial direction.

The absolute probe calibration is unknown at the 0.01% level. The manufacturer states that 0.1% precision is assured but that 0.01% precision requires yearly calibration. Since the magnetic measurements lasted several weeks, it is not clear what precision to expect. So a calibration parameter for each Hall probe was put into the fit. Note that since the NMR provides a very accurate absolute field measurement at the 0.1 gauss level, fitting for Hall probe calibrations cannot shift the overall field scale very much. For the B_ϕ probes, the field is small, and the offset was found to be more important than the calibration. Table 1 shows the calibration correction factors and offsets found by the fit.

Probe Number	1	2	3	4	5
Bz (factor)	-0.00015	0.00048	0.00026	0.00015	0.00018
Br (factor)	0.0071	0.0053	0.0041	0.0044	0.0044
B_ϕ (gauss)	2.35	-1.86			

Table 1. Calibration correction factors from the fit for the B_Z and B_R probes, and offset corrections for the B_ϕ probes.

The Z origin of the spindle and the phi origin of the propeller could change slightly during the process of moving the probe plate between data sets. These errors were found by fitting for four ΔZ and four $\Delta\phi$ parameters, one pair for each data set relative to data set 2. The fitted values are $\Delta Z=(0.3, 0., 0.2, 0.9, 0.3)\text{mm}$ and $\Delta\phi=(8.1, 0.0, -13.1, 33.1, -13.8)\text{mrad}$ for data sets (1, 2, 3, 2a, 3a) respectively.

Finally, the measured B_R and B_ϕ fields showed an irregular pattern versus phi at many Z and R points, as illustrated in Figure 6 and Figure 7 by the dotted data points. This irregularity was

most evident near the center ($Z=0$), and could not be explained by irregularities in the iron structure. It is most likely due to flexing of the propeller as it rotates about the spindle, changing the probe orientation at each phi setting. The magnitude of the irregularity, seen in the residuals from the fit, increases approximately linearly with the R coordinate. Corrections were made to the data for this flexure by adding parameters at each phi grid point for the change in orientation of the probes. This required 26 parameters for the R orientations (24 phi parameters and 2 parameters for the linear R dependence) and 26 similar parameters for the phi orientations. The corrected data points are considerably smoother after the flex corrections are applied, as shown by the plus signs in Figure 6 and Figure 7. The solid curves show the fits to the corrected data.

Br Field Distortions From Arm Flexure

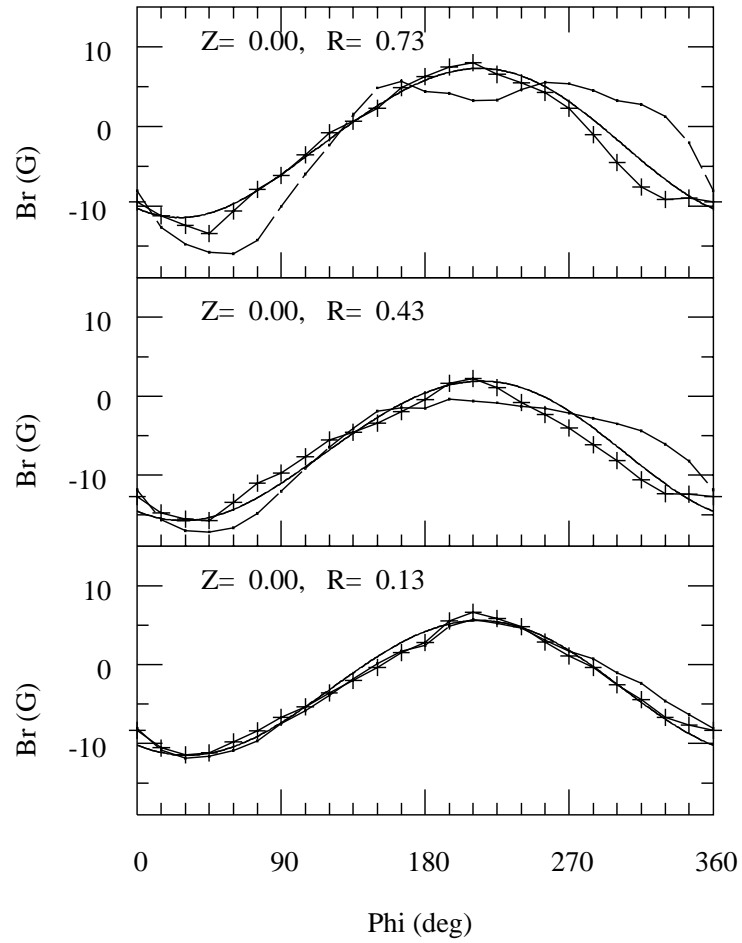


Figure 6. Distortions in the radial field component due to flexure in the probe arm as a function of ϕ . The distortion increases approximately linearly with the radial location of the radial probe. The dots show the data without any correction for the arm flexure, while the plus signs show the corrected data points. The solid curve is the fit to the corrected data points.

Bphi Field Distortions From Arm Flexure

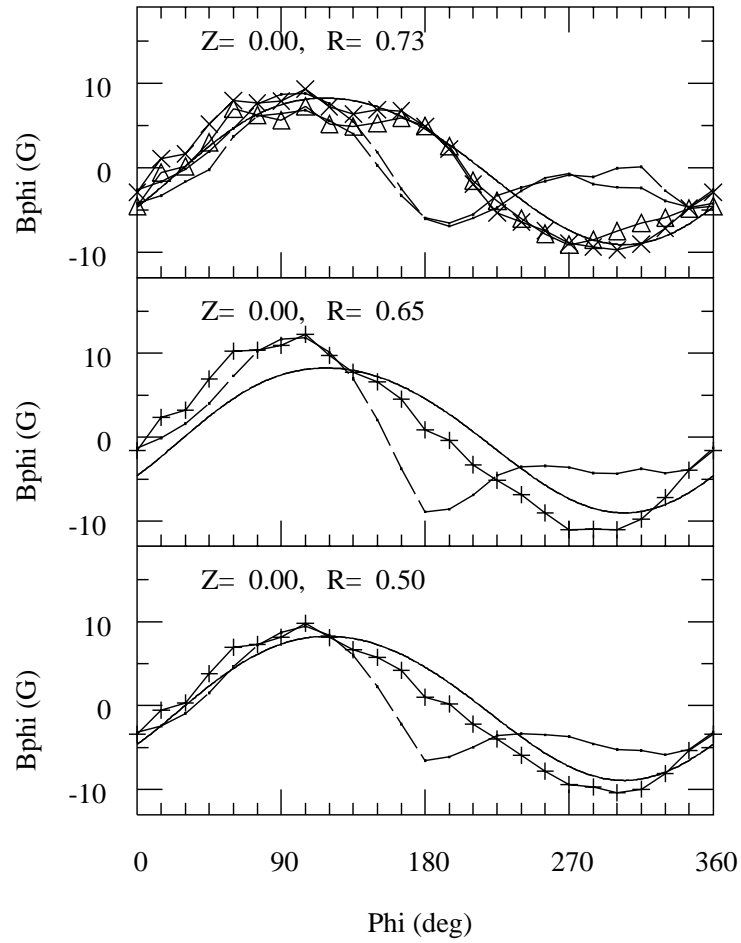


Figure 7. Distortions in the Bphi field component due to arm flexure, as described in the previous figure.

All of the above corrections were done by one routine (fixbdat) in an iterative manner. Values of the correction parameters were used to correct the data before the next fit iteration, and the fit in turn produced new correction parameters.

Magnetic Field Model

The equations for the magnetic field inside of the solenoid must satisfy Maxwell's equations. Since there are no magnetic sources within this volume, Maxwell's equations can be represented by a scalar potential satisfying the Laplace equation. The Laplace solutions are given in the next section for a cylindrical coordinate system based at the center of the solenoid. However, features such as holes in the BaBar iron end plates produce magnetic perturbations local to the end plate. It would require many terms to describe these perturbations by the centrally oriented Laplace solutions. These perturbations are better treated by functional terms located at each feature. These local functions (e.g. dipoles) are described in later sections.

The Scalar Magnetic Potential

The magnetic field in a source-free region can be described by a scalar magnetic potential ψ satisfying the Laplace equation

$$\nabla^2 \psi = 0.$$

When expressed in cylindrical coordinates, the solution $\psi(z, r, \phi)$ applicable to the inner volume of a solenoid is a linear combination of the following terms containing trigonometric, hyperbolic, and Bessel (I_n or J_n) functions,

$$\begin{aligned} & (s_1 \sin(n\phi) + c_1 \cos(n\phi)) \cdot \sin(kz) \cdot I_n(kr) \\ & (s_2 \sin(n\phi) + c_2 \cos(n\phi)) \cdot \cos(kz) \cdot I_n(kr) \\ & (s_3 \sin(n\phi) + c_3 \cos(n\phi)) \cdot \sinh(kz) \cdot J_n(kr) \\ & (s_4 \sin(n\phi) + c_4 \cos(n\phi)) \cdot \cosh(kz) \cdot J_n(kr) \end{aligned}$$

In these equations, n is an integer constant (0, 1, 2, ..), and $s_{1..4}, c_{1..4}, k$ are arbitrary constants. Any field can be described by a sum of terms, each having its own set of (s, c, n, k) constants.

The BaBar end plates have large holes along the axis for beam line components. These holes allow fields to extend in z outside of the end plates, with the fields decreasing at large z values. Field components with $\sin(kz)$ and $\cos(kz)$ terms are best suited to fit the decreasing field at large z , while terms with $\sinh(kz)$ or $\cosh(kz)$ that grow rapidly with z are not.

The Laplace potential function suitable for BaBar is then

$$\psi(z, r, \phi) = \sum_{n,i} \cos(n\phi - \phi_n) (s_{ni} \sin(k_{ni}z) + c_{ni} \cos(k_{ni}z)) \cdot I_0(k_{ni}r)$$

If the field is symmetric in ϕ , then n and ϕ_n can be set to zero in the above equations. This is mostly the case for the BaBar magnet. However, it is found that a few terms with n values of 1, 2, and 6 are also required for the best fits to the data.

The phi-symmetric Laplace potential function suitable for BaBar is

$$\psi(z, r) = \sum_i (s_i \sin(k_i z) + c_i \cos(k_i z)) \cdot I_0(k_i r)$$

Laplace Field Functions.

The magnetic fields are given by the gradients of the magnetic scalar potential, $\vec{B} = -\nabla \psi$. In cylindrical coordinates, these are

$$B_z(z, r, \phi) = -\frac{\partial \psi}{\partial z} \quad B_r(z, r, \phi) = -\frac{\partial \psi}{\partial r} \quad B_\phi(z, r, \phi) = -\frac{\partial \psi}{r \partial \phi}$$

The phi-symmetric field functions derived from the phi-symmetric Laplace potential function are

$$B_z(z, r) = \sum_i (s_i \cos(k_i z) - c_i \sin(k_i z)) \cdot I_0(k_i r)$$

$$B_r(z, r) = \sum_i (s_i \sin(k_i z) + c_i \cos(k_i z)) \cdot I_1(k_i r)$$

$$B_\phi(z, r) = 0.$$

These equations can be used to fit measured B_z, B_r, B_ϕ field values by choosing appropriate values for the k variables and fitting for the c coefficients. However, since the k values are arbitrary, it is difficult to pick an appropriate set that would minimize the number of terms required to fit the data. One attempt used the values $k_i = (i + 1)k_0$, with $k_0 \approx 0.5$ to match the approximate 2 meter detector size. It appeared that many terms were required to fit the data, and the computer time would be excessive.

An alternate method uses a set of polynomials to fit the data. Polynomials may be derived from the above set of equations by expanding each trigonometric or bessel term into a series, collecting terms of equal rank, and replacing the resulting factors $\sum s_i k_i^n$ and $\sum c_i k_i^n$ by new fitting parameters P_n . It is then simple to fit these parameters for as many terms as needed to describe the data to a certain level of accuracy. These derived polynomial field functions are shown in the following section.

Polynomial Field Functions.

The series expansion of the phi-symmetric Laplace field functions in the previous section gives the following polynomial field functions, shown for terms up to order n .

$$B_z(z, r) = \sum_{i=0}^n P_i \cdot (i!) \cdot (-1)^{\frac{i+1}{2}} \sum_{k=0(2)}^i \frac{(-1)^{k/2} z^{i-k} r^k}{(i-k)! \cdot 2^k \cdot ((k/2)!)^2}$$

$$B_r(z, r) = \sum_{i=1}^n P_i \cdot (i!) \cdot (-1)^{\frac{i+1}{2}} \sum_{k=1(2)}^i \frac{(-1)^{k/2} z^{i-k} r^k}{(i-k)! \cdot 2^k \cdot ((k/2)!)((k+1)/2)!}$$

$$B_\phi(z, r) = 0.$$

The $(i+1)/2$, $k/2$, and $(k+1)/2$ terms must be truncated to whole integers in the above expressions, and the k-summation is stepped by 2. Note that the same P_i fitting parameters appear in B_z and B_r in order to satisfy Maxwell's equations, since both equations are derived from the same magnetic potential.

The first few terms of each series are

$$B_z(z, r) = P_0 - P_1 z - P_2 \left(\frac{z^2}{2} - \frac{r^2}{4} \right) + P_3 \cdot 3 \left(\frac{z^3}{3} - \frac{zr^2}{2} \right) + \dots$$

$$B_r(z, r) = -P_1 \left(\frac{r}{2} \right) - P_2 (zr) + P_3 \cdot 3 \left(\frac{z^2 r}{2} - \frac{r^3}{8} \right) + \dots$$

$$B_\phi(z, r) = 0.$$

It was found that the fit was improved by using terms up to P_{40} .

Phi Dependent Fields.

The BaBar magnet iron is not phi symmetric because of the holes and other features shown in Figures 1 and 2, requiring that phi dependent field terms be added to the fitting model. These phi asymmetric features in the doors and barrel iron are:

1. The iron at the bottom region of the backward end plate has through holes for cable access and for the rails and lead screws of the plug removal mechanism.
2. The backward end plate has a vertically running channel at the top portion for services to the liquid helium cryostat.
3. Both front and back end plates are not solid iron but consist of many parallel plates of iron spaced apart for the RPC detectors. Iron spacers along the door boundaries and interior parts keep the plates separated, but these

spacers also cause localized magnetic field concentrations on the end plate faces.

4. The front doors have vertically running channels at the top half where iron has been removed at the closing surfaces.
5. One of the front doors became warped during manufacture and was straightened by removing iron from the warped face.
6. The barrel iron has a hexagonal shape, which gives rise to distortion with six-fold symmetry at large radii.
7. Each hexagonal side in the barrel iron has access slots for cables, which distorts the field at large r and large z.

In order to fit the phi-dependent fields, other functional terms were added to the field model.

A magnetic dipole term oriented along the Z-axis at each hole on the end plate gives an approximate representation of the field from the missing magnetized iron.

For extended objects such as the linear RPC spacers, a rectangular shaped pole was used instead. A rectangular pole is achieved by placing a rectangular loop of current in the plane of the end plate that circumvents the object, giving a pole pointing along the z-axis over the length of the rectangle.

The asymmetry due to the warped doors can be modeled in part by an annular dipole of varying width along its circumference. An annular dipole consists of two current loops in the plane of the end plate having opposite currents and origins slightly displaced from each other.

The functional forms for these phi-dependent fields are given in the following sections.

Field Equations of a Point Dipole

For a point dipole of strength M oriented along the z direction at coordinate (z_d, r_d, ϕ_d) , the field components seen at point (z, r, ϕ) are

$$B_z = M \frac{3(z - z_d)^2 - \rho^2}{\rho^5}$$

$$B_r = 3M \frac{(z - z_d)(r - r_d \cos(\phi - \phi_d))}{\rho^5}$$

$$B_\phi = 3M \frac{(z - z_d)(r_d \sin(\phi - \phi_d))}{\rho^5},$$

where $\rho^2 = r^2 + r_d^2 - 2rr_d \cos(\phi - \phi_d) + (z - z_d)^2$.

Field Equations of a Rectangular Pole

The field from a rectangular current loop of I amperes can be calculated analytically from the fields of four linear current segments along the sides $y = y_1$, $x = x_2$, $y = y_2$, and $x = x_1$ in the plane $z = z_d$. The field equations in rectangular coordinates are

$$\begin{aligned} B_x &= C(z - z_d) \{G(y, y_1, y_2, \rho_2) - G(y, y_1, y_2, \rho_4)\} \\ B_y &= C(z - z_d) \{-G(x, x_1, x_2, \rho_1) + G(x, x_1, x_2, \rho_3)\} \\ B_z &= C \left\{ \begin{aligned} (y - y_1)G(x, x_1, x_2, \rho_1) - (x - x_2)G(y, y_1, y_2, \rho_2) \\ - (y - y_2)G(x, x_1, x_2, \rho_3) + (x - x_1)G(y, y_1, y_2, \rho_4) \end{aligned} \right\} \end{aligned}$$

These can be transformed into cylindrical coordinates, as

$$\begin{aligned} B_r &= B_x \cos(\phi) + B_y \sin(\phi) \\ B_\phi &= -B_x \sin(\phi) + B_y \cos(\phi) \end{aligned}$$

where $C = \frac{\mu_0 I}{4\pi}$

$$G(\eta, \eta_1, \eta_2, \rho) = \frac{\tanh(\sinh^{-1}((\eta - \eta_2)/\rho)) - \tanh(\sinh^{-1}((\eta - \eta_1)/\rho))}{\rho^2}$$

$$\rho_1^2 = (y - y_1)^2 + (z - z_d)^2$$

$$\rho_2^2 = (x - x_2)^2 + (z - z_d)^2$$

$$\rho_3^2 = (y - y_2)^2 + (z - z_d)^2$$

$$\rho_4^2 = (x - x_1)^2 + (z - z_d)^2$$

Fields From Annular Pole

An annular pole consists of two concentric current loops with currents running in opposite directions and the loop origins slightly displaced from each other. The field along the circumference midway between the two loops will point along the z direction, and will vary in a sinusoidal pattern along the circumference.

The field components at point (r, ϕ, z) from one circular loop of current I centered at $(0, 0, z_c)$ with radius r_c in the x, y plane are shown below. The solutions have two elliptical integrals, defined here as

$$F_0(\alpha) = \oint \frac{d\theta}{(1 - \alpha \cos(\theta))^{3/2}}, \quad F_1(\alpha) = \oint \frac{\cos(\theta) d\theta}{(1 - \alpha \cos(\theta))^{3/2}}$$

The field components are

$$B_r = \frac{I(z - z_c)}{d^3} F_1(\alpha) \cos(\phi)$$

$$B_\phi = \frac{I(z - z_c)}{d^3} F_1(\alpha) \sin(\phi)$$

$$B_z = \frac{I}{d^3} \{r_c F_0(\alpha) - r F_1(\alpha)\}$$

where

$$d = \sqrt{r^2 + r_c^2 + (z - z_c)^2}$$

$$\alpha = \frac{2r_c r}{d^2}$$

The field components from an annular pole are obtained by adding the fields from two circular loops of slightly displaced origins with opposite I signs.

Other Phi Dependent Fields

The barrel iron surrounding the solenoid coil is in the shape of a hexagon, so a field component with six-fold symmetry in phi would be expected at large radii. This six-fold asymmetry can be modeled with a few trigonometric-bessel terms (with n=6) added to the fitting model.

It was also found necessary to include trigonometric-bessel terms with n=2 and n=1. The source for these fields is not precisely known, but a slightly flattened hexagonal barrel would give an n=2 component, while a slightly off-centered component (coil or iron) could give an n=1 component.

Fitting Procedure

A non-linear least squares fitting program[4] was used to fit the model to the measured data. The fit varied parameters pertaining to the model as well as parameters that were corrections to the measured data. Some derivatives were computed analytically to reduce the computation time. The data from all good probes in all data sets (46320 total points) were used in the fit, and a fit took anywhere from 1 to 15 hours of RS6000 computer time, depending on the number of parameters in the fit. A command script was developed to allow selection of parameters in the fit, correction factors to be applied, plots to be made, and save and restore a configuration by the fitting job - mapcmd.

An assumed error of measurement of the probes for data points within the drift chamber tracking volume was as follows:

- NMR: 0.1 gauss
- B_Z Hall probes: 1.0 gauss
- B_R Hall probes: 1.0 gauss
- B_φ Hall probes: 3.0 gauss

Because of the difficulty in modeling the field near the non-uniform iron, the assigned errors were increased (doubled) for points outside the tracking volume, and doubled again for the outer-most grid points in Z and R.

Choice of fitting functions and parameters

The functional elements described previously in the magnetic field model were included the fit. The number and placement of some of the elemental components such as the point dipoles for the holes and rectangular dipoles for the IFR spacer was straightforward. However, some of the elemental parameters like the number of polynomial terms or the placement of annular dipoles at the front door had to be determined by trial and error for best results (i.e. a decrease in χ^2 and improvement in residuals in the region of interest). The results of these trials, and of fits with and without certain elements, are summarized here.

Fits were done with a varying number of polynomial terms to establish the minimum number that need be used. The χ^2 per degree of freedom decreases with the number of polynomial terms below 40 terms, with little improvement beyond that as shown in Table 2. Forty terms were used in the final fits.

# Polynomial Terms	Chi2/DF
15	53.50
20	26.80
25	6.93
30	3.97
35	3.16
40	2.89
50	2.87

Table 2. The χ^2 per degree of freedom as a function of the number of polynomial terms used in the fit. The fit improves with more terms up to 40, and little improvement beyond that.

Establishing the number of other functional elements and their parameters (e.g. coordinates and strengths of dipoles, coordinates, strengths, and area of rectangular poles, number of Bessel elements, etc.) required numerous fits to be done, adding a few components at a time. Some fits with selected components turned off are shown in Appendix C for the interested reader.

The final configuration included 80 fitting parameters, as follows:

- 4 Magnetic axis terms ($X_0, Y_0, \theta_{XZ}, \theta_{YZ}$)
- 40 polynomial strengths
- 1 Bessel (n=1) strength
- 2 Bessel (n=2) strengths
- 3 Bessel (n=6) strengths
- 9 Dipole strengths, some lumped together (22 total)
- 14 Rectangular pole strengths, some lumped together (20 total)
- 7 Annular pole strengths

The locations of all the poles on the front and rear end plates are shown graphically in Figure 8 and Figure 9 respectively.

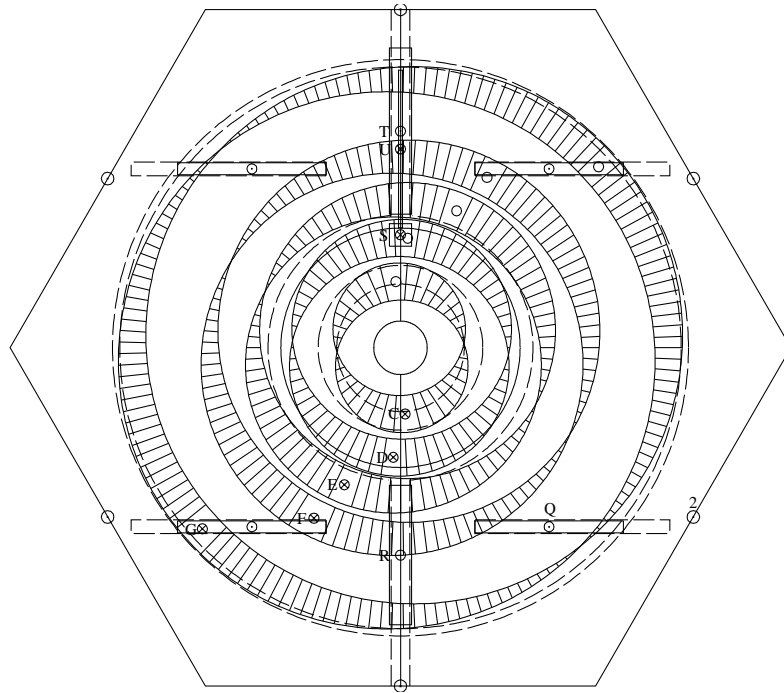


Figure 8 shows the locations of rectangular and annular poles on the front end plate. The pole numbers refer to the parameter names shown in Appendix B.

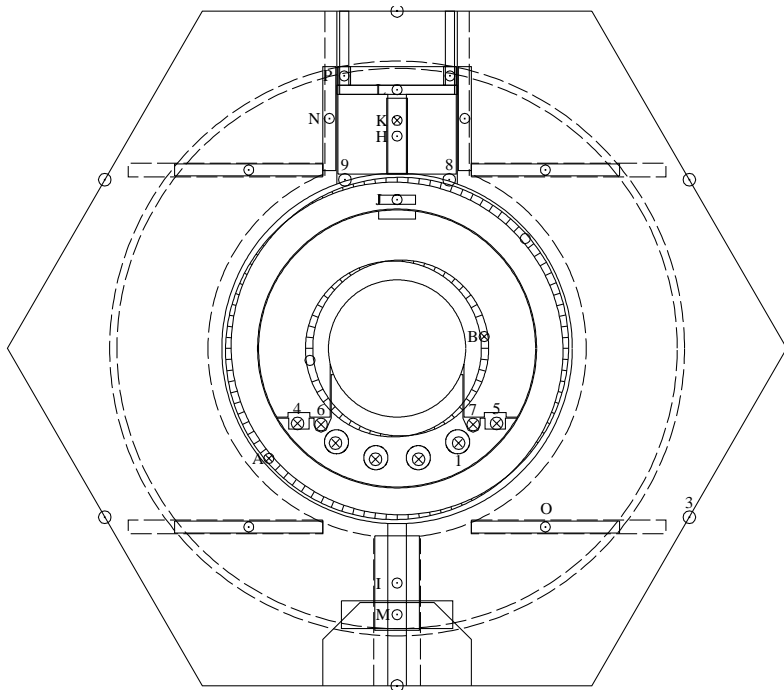


Figure 9 shows the locations of all poles on the rear end plate. The pole numbers refer to the parameter names shown Appendix B.

Results

The numerical values of the 80 fitted parameters, as well as other static parameters, are shown in Appendix B. Fitted parameters have non-zero values in the Sigma field. Names beginning with “P” are polynomial terms, “D” are dipole terms, “L” are annular (Loop) poles, and “S” are (Segmented) rectangular poles.

Not shown in Appendix B are the correction parameters. These corrections were found by other fits, and the parameters were copied into the subroutine (fixbdat) so that corrections to the data could be made in subsequent fits.

A χ^2 per degree of freedom of 2.89 is found in the final fit. This implies that the model is not yet complete, or that the assumed measuring errors (e.g. 1.0 gauss for BZ probes) enumerated previously are too small, or some combination of the two. Increasing all the measuring errors by a factor of 1.7 is well within the estimate of the probe precision, and doing so would give the ideal fit with a χ^2 per degree of freedom of 1.0.

The root mean square of the residuals is 1.7 gauss for points within the tracking fiducial volume and 4.8 gauss for all the measured points.

Examples of the corrected measurements superimposed with the fitted curves for the B_Z and B_R fields versus Z at $\phi=0$ are shown in Figure 10 and Figure 11.

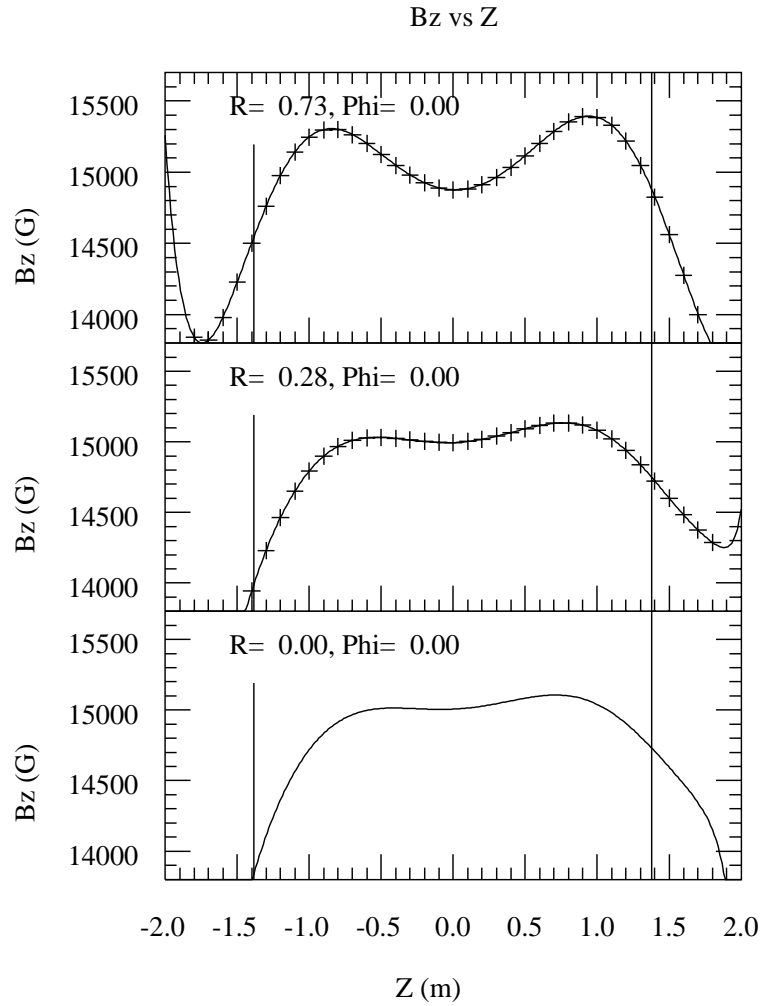


Figure 10. The B_z field is shown as a function of Z at three values of R with $\varphi=0$. The plus signs show the corrected data points while the solid lines come from the fitted model. The vertical lines at $Z=-1.4\text{m}$ and $Z=1.4\text{m}$ show the drift chamber bounds along the Z coordinate. The top plot shows the field at $R=0.73$ (between super layer 9 and 10), the middle plot is at $R=0.28$ (middle of super layer 1), and the bottom plot is at $R=0$ along the axis of the chamber.

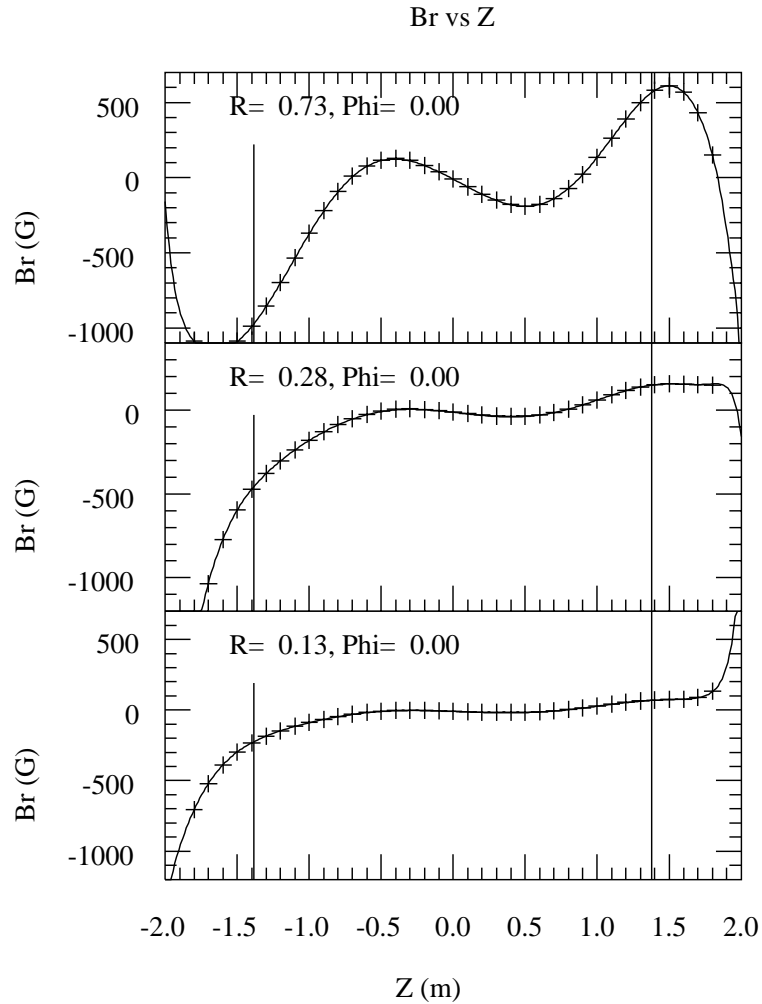


Figure 11. Shows the Br field as a function of Z, with similar conditions as in the previous figure.

While the previous figures show the fields at a few locations in the drift chamber, it is more useful to know the fields along a trajectory of a track to estimate errors in track parameters from the non-uniform magnetic field. The next two figures show the fields along infinitely high momentum tracks having production angles θ of 18, 25, 55, and 140 degrees to the +Z axis. The Bz and Br fields are shown at an azimuth angle ϕ of 0 degrees. The maximum Bz variation over the chamber length is approximately 1000 gauss (6.7%) at all radii. The maximum Br variation is 1700 gauss at R=0.73m. The magnitude of the $B\phi$ variation (not shown) is much less, but it varies rapidly with the ϕ angle in the vicinity of 90 and 270 degrees.

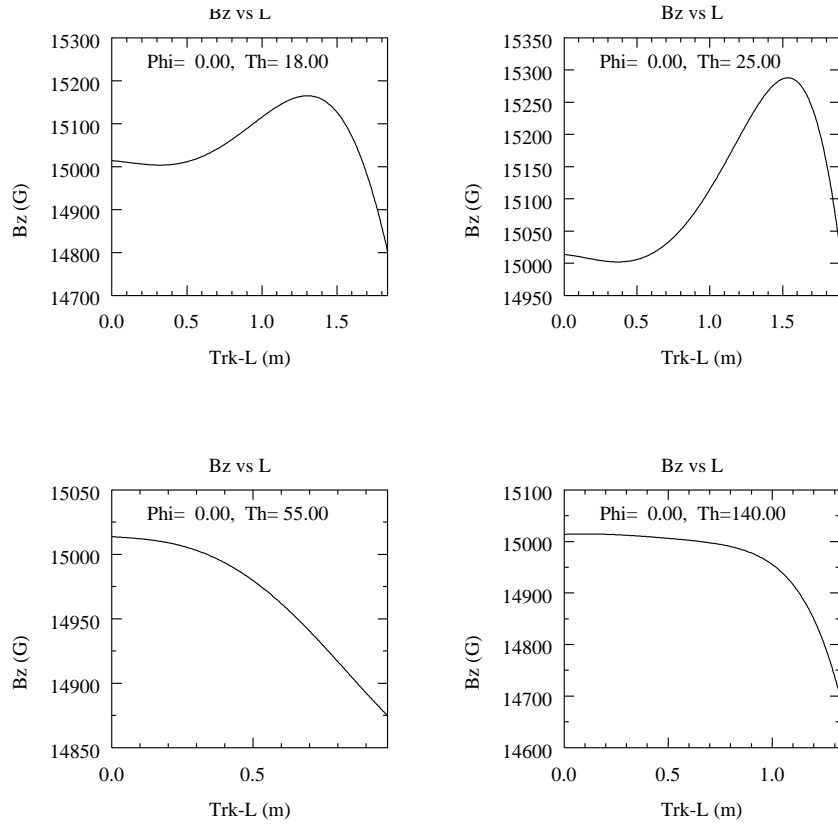


Figure 12. Values of B_z along a straight track originating at the interaction point and terminating at the drift chamber outer wall or an end plate. The four graphs are for tracks at production angles $\theta = 18, 25, 55,$ and 140 degrees. The maximum variation in B_z is approximately 300 gauss near the end of the track when $\theta = 25^\circ$.

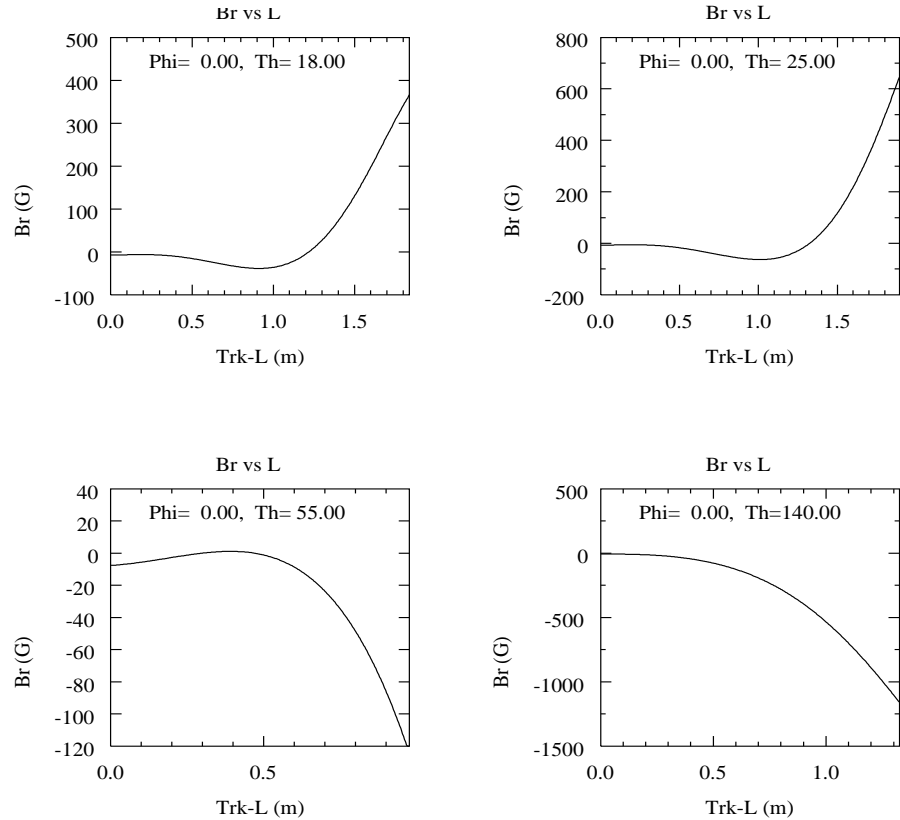


Figure 13. Values of Br along a straight track originating at the interaction point and terminating at the drift chamber outer wall or an end plate. The four graphs are for tracks at production angles $\theta = 18, 25, 55,$ and 140 degrees. The maximum variation in Br is approximately 600 gauss at the end of the track when $\theta = 25^\circ$, and 1300 gauss when $\theta = 140^\circ$.

Conclusions

The magnetic mapping data for the BaBar solenoid magnet has been fitted with a model containing polynomial terms for the coil field, and Bessel/trigonometric terms, dipoles, and other loops of currents that provide local field perturbations from the non-uniform distribution of iron on the end plates. The data and the model agree to 1.7 gauss (RMS) for grid points within the tracking volume of the drift chamber, and to 4.8 gauss for the full measured volume ($|Z| < 1.8\text{m}$, $R < 1.3\text{m}$).

The modeling and fitting software used in this report reside in the SLAC unix file system in the `~adam/magfit` directory. The code is in Fortran. The following source files are used by the modeling software – `bmap_func.f`, `dbsja.f`, `b_rect.f`, and `bloop.f`. A block data file `bmap_block.cmn` provides the fitted parameters, and include-files `bmap_parm.cmn`, `bmulti.cmn` are also required. Comments in `bmap_func.f` provide the calling sequence for the function.

The above source files have also been combined with the model for the fringe fields from the beam line components[1]. The latter files reside on SLAC unix in the

~wmd/bbmagnet/bbmagfield directory. A source file bbmagfields.f in this directory provides the total field by calling both the solenoid and the fringe field subprograms. An argument in bbmagfields determines whether the field is calculated by the functions, or interpolated from a stored grid of field values. The latter method uses less computer time. The grid point values are computed from the functions at grid spacings of 10mm in Z and R within the tracking volume, and at 50mm spacing beyond the tracking volume. Linear interpolation is used for the 10mm grid points, and quadratic interpolation is used for the coarser 50mm grid. The phi variation in the three field components is provided by 5 to 36 pre-determined Fourier coefficients that have been found from analyses of the solenoid field functions.

Acknowledgements

We acknowledge the valuable help from Stepen Mikhailov in calculating the field predictions for BaBar using the MERMAID computer program.

Appendix A. Data Runs

Data Set	Pos	B (T)	Run	Z (m) of Phi-Swaths in the Run	Bad Probes
2	2	1.5	27	-1.8, -1.7, -1.6	
			28	-1.5, -1.4	
			29	-1.2, -1.0, -0.8	
			30	-0.6, -0.4, -0.2	
			31	0.0, 0.2, 0.4	
			32	0.6, 0.8, 1.0	
			34	1.2, 1.4	
			35	1.5, 1.6, 1.7, 1.8	
			2L	2	
43	-1.6, -1.5, -1.4				
44	-1.2, -1.0, -0.8				
45	-0.6, -0.4, -0.2				
48	0.0, 0.2, 0.4, 0.6				
49	0.8, 1.0, 1.2, 1.4				
50	1.5, 1.6, 1.7, 1.8				
3	3	1.5	52	-1.8, -1.7, -1.6, -1.5	
			53	-1.4, -1.3	
			55	-1.2, -1.1, -1.0, -0.9	
			58	-0.8, -0.7, -0.6, -0.5	
			59	-0.4, -0.3, -0.2, -0.1	
			60	0.0, 0.1	
			61	0.2, 0.3, 0.4, 0.5	
			62	0.6, 0.7, 0.8, 0.9	
			63	1.0, 1.1, 1.2, 1.3	
			64	1.4, 1.5, 1.6, 1.7, 1.8	
3a	3	1.5	67	-1.8, -1.7, -1.6, -1.5, -1.4, -1.3, -1.2, -1.1	Bz3
			68	-1.0, -0.9, -0.8, -0.7, -0.6, -0.5, -0.4, -0.3	Bz3
			69	-0.2, -0.1, 0.0, 0.1, 0.2, 0.3, 0.4, 0.5	Bz3
			70	1.2, 1.3	Bz3
			72	0.6, 0.7, 0.8, 0.9, 1.0, 1.1	Bz3
			73	1.4, 1.5, 1.6, 1.7, 1.8	Bz3
3L	3	1.0	75	-1.8, -1.7, -1.6, -1.5, -1.4, -1.3, -1.2, -1.1	Bz3
			76	-1.0, -0.9, -0.8, -0.7, -0.6, -0.5, -0.4, -0.3	Bz3
			77	-0.2, -0.1, 0.0, 0.1, 0.2, 0.3, 0.4, 0.5	Bz3
			78	0.6, 0.7, 0.8, 0.9, 1.0, 1.1, 1.2, 1.3	Bz3
			79	1.4, 1.5, 1.6, 1.7, 1.8	Bz3
1	1	1.5	81	-1.8, -1.7, -1.6, -1.5, -1.4, -1.3, -1.2, -1.1	Bz3, Bz4
			82	-1.0, -0.9, -0.8, -0.7, -0.6, -0.5, -0.4, -0.3	Bz3, Bz4
			83	-0.2, -0.1, 0.0, 0.1, 0.2, 0.3, 0.4, 0.5	Bz3, Bz4
			84	0.6, 0.7, 0.8, 0.9, 1.0, 1.1, 1.2, 1.3	Bz3, Bz4
			85	1.4, 1.5, 1.6, 1.7, 1.8	Bz3, Bz4
2a	2	1.5	87	-1.8, -1.7, -1.6, -1.5, -1.4, -1.3, -1.2, -1.1	Bz3, Bz4
			88	-1.0, -0.9, -0.8, -0.7, -0.6, -0.5	Bz3, Bz4
			89	-0.4, -0.3, -0.2, -0.1, 0.0	Bz3, Bz4
			90	0.1, 0.2, 0.3, 0.4, 0.5, 0.6	Bz3, Bz4
			91	0.7, 0.8, 0.9, 1.0, 1.1, 1.2	Bz3, Bz4
			92	1.3, 1.4, 1.5, 1.6, 1.7, 1.8	Bz3, Bz4

This table shows the data runs taken. Columns 1 through 6 show the Data Set name, the Plate Position, the nominal field in Tesla, the run number, the contents of the run (Z values), and finally a list of bad probes occurring in the run.

Appendix B. Fit Parameters

The parameters from the final fit are listed below. Of the 203 parameters, 80 were varied in the fit. Static parameters are identified by the zero value in the "Fitted Sigma" field. Parameter Names beginning with "P" are polynomial coefficients, "D" are dipoles strengths, "L" are annular Loop strengths, and "S" are Segmented rectangular poles. The locations of the dipoles, current loops, and rectangular poles can be seen in Figure 8 and Figure 9. The Chi-Square per degree of freedom is 2.89 using the errors of measurement given in the text.

==== B-field fit, 203 parameters, 80 fitted =====

Using: O= 5 P=40 B=20 D= 3 6 0 7 14 0 A= 0 C= 0 Dz= 0 Dp= 0 v=1 R= 81 .. 73

CH2/DF = 0.1338E+06 / 46240. = 2.89 Std Dev = 1.70

Parm#	Name	Fitted Value	Fitted Sigma
1	Z0	0.00000	0.00000
2	X0	0.197672E-02	0.111016E-04
3	Y0	-0.481347E-04	0.123382E-04
4	XA	-0.671059E-03	0.116408E-05
5	YA	-0.381695E-03	0.148168E-05
6	P0	15017.1	0.998195E-01
7	P1	52.6397	0.488043E-01
8	P2	-302.703	0.821237E-01
9	P3	-107.716	0.365522E-01
10	P4	-481.214	0.310625E-01
11	P5	5.93199	0.255469E-01
12	P6	-68.6686	0.241462E-01
13	P7	0.349665	0.215695E-01
14	P8	19.4623	0.189233E-01
15	P9	4.81760	0.162894E-01
16	P10	11.6971	0.138093E-01
17	P11	0.476194	0.115824E-01
18	P12	1.79045	0.954281E-02
19	P13	-0.596731E-01	0.783118E-02
20	P14	-0.210750	0.619455E-02
21	P15	-0.144900	0.495477E-02
22	P16	-0.331542	0.367270E-02
23	P17	-0.558871E-01	0.284690E-02
24	P18	-0.127491	0.192962E-02
25	P19	-0.344597E-02	0.144461E-02
26	P20	-0.227639E-01	0.878650E-03
27	P21	0.718395E-02	0.634974E-03
28	P22	0.254295E-02	0.341950E-03
29	P23	0.501637E-02	0.238858E-03
30	P24	0.354775E-02	0.112675E-03
31	P25	0.203471E-02	0.762408E-04
32	P26	0.147176E-02	0.311788E-04
33	P27	0.614303E-03	0.204847E-04
34	P28	0.413303E-03	0.716834E-05
35	P29	0.144535E-03	0.458356E-05
36	P30	0.875690E-04	0.134971E-05
37	P31	0.270296E-04	0.841580E-06
38	P32	0.141098E-04	0.202720E-06
39	P33	0.394015E-05	0.123482E-06
40	P34	0.173790E-05	0.234006E-07
41	P35	0.438519E-06	0.139379E-07
42	P36	0.144725E-06	0.188619E-08
43	P37	0.335611E-07	0.110002E-08
44	P38	0.790830E-08	0.917873E-10
45	P39	0.157205E-08	0.522016E-10
46	lamda1	4.00000	0.00000

47	besphi1	1.68240	0.00000
48	besicz1	-225.675	0.912316
49	besisz1	0.00000	0.00000
50	lamda2	0.496580	0.00000
51	besphi2	0.593800E-01	0.00000
52	besjcz2	5.31312	0.133297E-01
53	besjsz2	0.864580	0.124649E-01
54	lamda6	0.343000	0.00000
55	besphi6	0.280600	0.00000
56	besicz6	-21.7013	0.330835
57	besisz6	0.00000	0.00000
58	lamda6	0.686000	0.00000
59	besphi6	-0.694570	0.00000
60	besicz6	-745.432	29.1964
61	besisz6	0.00000	0.00000
62	lamda6	0.343000	0.00000
63	besphi6	-0.126000E-01	0.00000
64	besjcz6	-0.882865	0.295023E-01
65	besjsz6	0.00000	0.00000
66	D1	-1.81297	0.633806E-02
67	D1z3	-2.19200	0.00000
68	D1H	0.648700	0.00000
69	D2	23.8128	0.225622
70	D2z	2.00000	0.00000
71	D2a	1.82000	0.00000
72	D3	17.9042	0.228598
73	D3z	-2.00000	0.00000
74	D3a	1.82000	0.00000
75	D4	-2.17741	0.449752E-01
76	D4z	-2.16500	0.00000
77	D4r	0.672000	0.00000
78	D4p	3.78740	0.00000
79	D5	-1.16987	0.408228E-01
80	D5z	-2.16500	0.00000
81	D5r	0.672000	0.00000
82	D5p	5.63740	0.00000
83	D6	-0.223803E-02	0.494879E-01
84	D6z	-2.16500	0.00000
85	D6r	0.580000	0.00000
86	D6p	3.92700	0.00000
87	D7	-0.213299	0.466361E-01
88	D7z	-2.16500	0.00000
89	D7r	0.580000	0.00000
90	D7p	5.49800	0.00000
91	D8	14.0481	0.198160
92	D8z	-2.30500	0.00000
93	D8r	0.952000	0.00000
94	D8p	1.27080	0.00000
95	D9	12.7278	0.196172
96	D9z	-2.30500	0.00000
97	D9r	0.952000	0.00000
98	D9p	1.87080	0.00000
99	LA	77319.7	669.418
100	LAz	-2.30200	0.00000
101	LAr	0.909800	0.00000
102	LAp	3.85029	0.00000
103	LAdr	0.200000E-01	0.00000
104	LB	25651.4	391.932
105	LBz	-2.14390	0.00000
106	LBr	0.474284	0.00000
107	LBP	0.134779	0.00000
108	LBdr	0.200000E-01	0.00000
109	LC	-24375.5	92.9083
110	LCz	2.10000	0.00000
111	LCr	0.356608	0.00000
112	LCp	4.78271	0.00000
113	LCdr	0.100000	0.00000
114	LD	-10384.6	53.0628
115	LDz	2.00000	0.00000
116	LDr	0.590711	0.00000
117	LDp	4.64667	0.00000

118	LDdr	0.100000	0.00000
119	LE	-10761.1	43.3804
120	LEz	2.00000	0.00000
121	LEr	0.795972	0.00000
122	LEp	4.32318	0.00000
123	LEdr	0.100000	0.00000
124	LF	-7163.28	58.2716
125	LFz	2.00000	0.00000
126	LFr	1.02803	0.00000
127	LFp	4.24203	0.00000
128	LFdr	0.100000	0.00000
129	LG	-59019.9	223.682
130	LGz	2.50000	0.00000
131	LGr	1.44447	0.00000
132	LGp	3.88172	0.00000
133	LGdr	0.100000	0.00000
134	SH	616.786	5.69295
135	SHz	-2.15000	0.00000
136	SHy	0.940000	0.00000
137	SHw	0.550000E-01	0.00000
138	SHh	0.410000	0.00000
139	SI	107.235	0.538636
140	SIz	-2.15000	0.00000
141	SIy	-1.01000	0.00000
142	SIw	0.120000	0.00000
143	SIh	0.510000	0.00000
144	SJ	1727.66	14.9564
145	SJz	-2.27319	0.00000
146	SJy	0.777724	0.00000
147	SJw	0.100000	0.00000
148	SJh	0.497000E-01	0.00000
149	SK	-406.889	2.71231
150	SKz4	-2.30749	0.00000
151	SKy	0.940000	0.00000
152	SKwv	0.320000	0.00000
153	SKh	0.580000	0.00000
154	SL	1837.65	13.6693
155	SLz4	-2.24300	0.00000
156	SLy	1.37000	0.00000
157	SLwv	0.324000	0.00000
158	SLh	0.500000E-01	0.00000
159	SM	21.1862	0.745042
160	SMz	-2.05700	0.00000
161	SMy	-1.36000	0.00000
162	SMw	0.300000	0.00000
163	SMh	0.150000	0.00000
164	SND	1075.95	8.50194
165	SNz	-2.25400	0.00000
166	SNy	0.960000	0.00000
167	SNw	0.400000	0.00000
168	SNh	0.560000	0.00000
169	SOQ	69.6871	0.649493
170	SOz	-2.10000	0.00000
171	SOy	0.930000	0.00000
172	SOw	1.20000	0.00000
173	SOh	0.650000E-01	0.00000
174	SPD	195.800	49.7238
175	SPz	-2.25000	0.00000
176	SPy	1.42000	0.00000
177	SPw	0.320000	0.00000
178	SPh	0.100000	0.00000
179	SQQ	31.4133	0.211683
180	SQz	1.98100	0.00000
181	SQy	0.930000	0.00000
182	SQw	1.20000	0.00000
183	SQh	0.650000E-01	0.00000
184	SR	116.783	0.341392
185	SRz	2.09300	0.00000
186	SRy	-0.740000	0.00000
187	SRw	0.600000E-01	0.00000
188	SRh	0.750000	0.00000

189	SS	-14693.9	38.3678
190	SSz	2.90446	0.00000
191	SSy	0.547278	0.00000
192	SSw	0.600000E-01	0.00000
193	SSh	0.120000	0.00000
194	ST	134.315	1.13588
195	STz	2.09300	0.00000
196	STy	0.718484	0.00000
197	STw	0.600000E-01	0.00000
198	STh	0.894134	0.00000
199	SU	-402.330	3.60762
200	SUz	2.02000	0.00000
201	SUy	0.644000	0.00000
202	SUw	0.100000E-01	0.00000
203	SUh	0.850000	0.00000

Appendix C. Fit Components

Table 3 gives the χ^2 per degree of freedom for the full fit as well as fits that have one major element group removed from the full set. The table also gives the parameters of the magnetic axis for each case. The cases shown below are fits with the full number of parameters but not including:

- The magnetic axis parameters - X_0 , Y_0 , θ_{XZ} , θ_{YZ} , one Bessel($n=1$) term
- 2 – Bessel($n=2$) terms
- 3 - Bessel($n=6$) terms
- 5 - annular poles and 1 rectangular pole at the front end plate
- 8 – plug rails and cable way holes at the rear end plate
- 5 – rectangular poles, 2 – dipoles, for cryogenic channel at the rear end plate
- 8 – rectangular poles for IFR spacers (front and rear)

The χ^2 value changes significantly in all case except f). However, the residuals for case f) are smaller in the vicinity of the cryogenic channel (Figure 19), so these elements are retained in the final fit.

Case	Model Parameters	Chi2/DF	X0 (mm)	Y0 (mm)	ThetaX (mrad)	ThetaY (mrad)
	Full fit	2.89	2.0	0.0	-0.67	-0.38
a	Full - axes	13.40	0.0	0.0	0.00	0.00
b	Full - Bessel n=2	9.00	2.2	0.7	-0.74	-0.35
c	Full - Bessel n=6	4.00	2.0	0.0	-0.68	-0.37
d	Full - front annular poles	9.25	0.8	0.0	-0.41	-0.36
e	Full - rear plug holes	6.37	2.2	-0.3	-0.67	-0.16
f	Full - rear flue channel	2.90	2.0	-0.3	-0.69	-0.32
g	Full - IFR spacers	3.60	1.9	-0.2	-0.67	-0.42

Table 3 shows the results of fits when one of the model elements is removed. The χ^2 and coordinates of the magnetic axis are shown for the full fit and fits without the axis, without the dipole terms for holes in the plug, etc. in the fit.

Figure 14 through Figure 20 show plots of the data and the fits for the cases a) to g) in Table 3 in a region of Z and R that best illustrates the effects of removing the component from the fit. The solid line is the full fit, while the dashed line shows the fit without the component. The model agrees better with the data in all cases when the component is included in the fit.

Field Distortions From Misaligned Axes

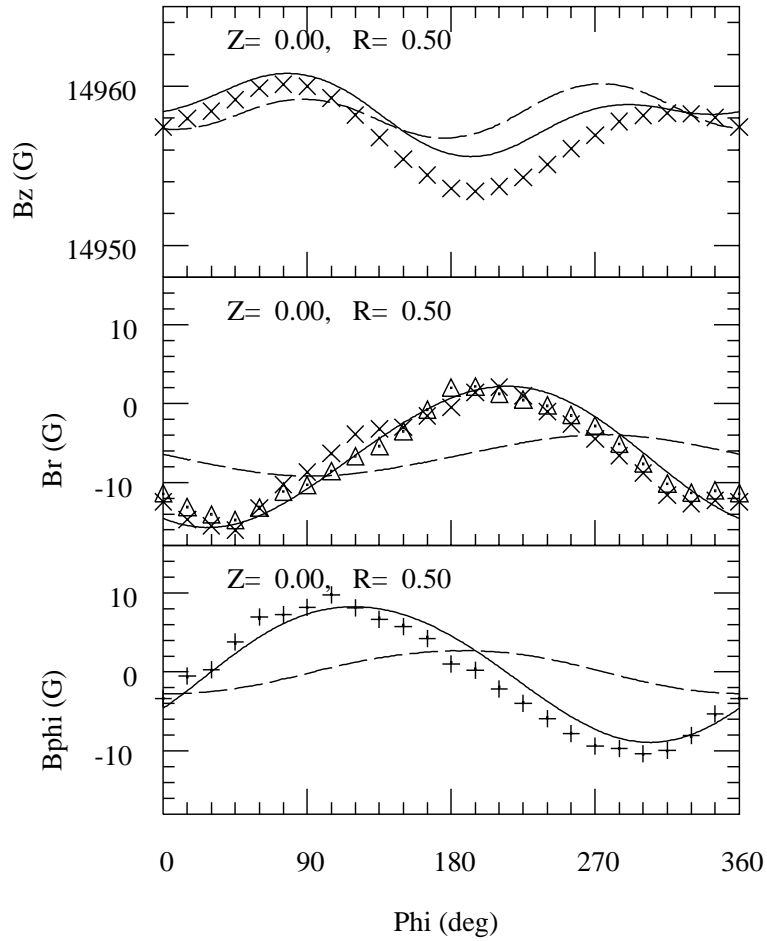


Figure 14. Case a). The three field components (B_z , B_r , and B_{ϕ}) as a function of ϕ at the center of the magnet at $R=0.50\text{m}$. The sinusoidal nature of the data for B_r and B_{ϕ} arises from the misalignment of field axis from the detector axis by -0.67mrad in the X-Z plane and by -0.38mrad in the Y-Z plane. The solid curve is a full fit to the data, and the dashed curve is a fit without axis parameters.

N=2 Bessel Term Contribution

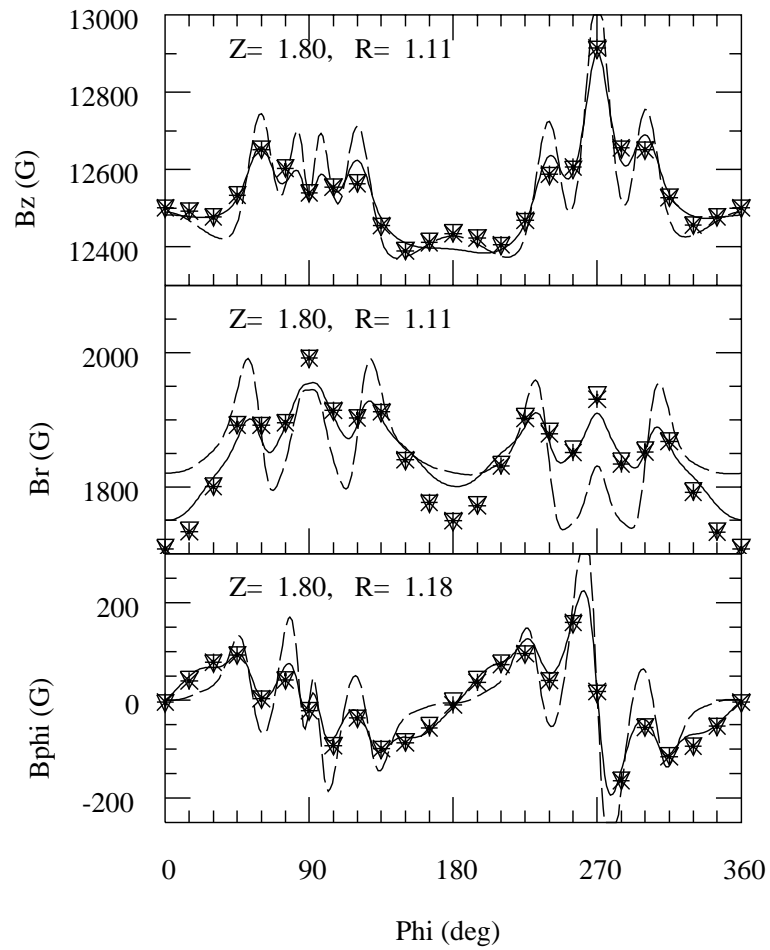


Figure 15. Case b). The field components near the front end plate at $R=1.11\text{m}$ showing the fit with (solid lines) and without (dashed lines) the $n=2$ Bessel terms. The broad enhancements in the data at approximately 90 and 270 degrees is described by the $n=2$ term in the fit.

6-Fold Symmetric Field Terms

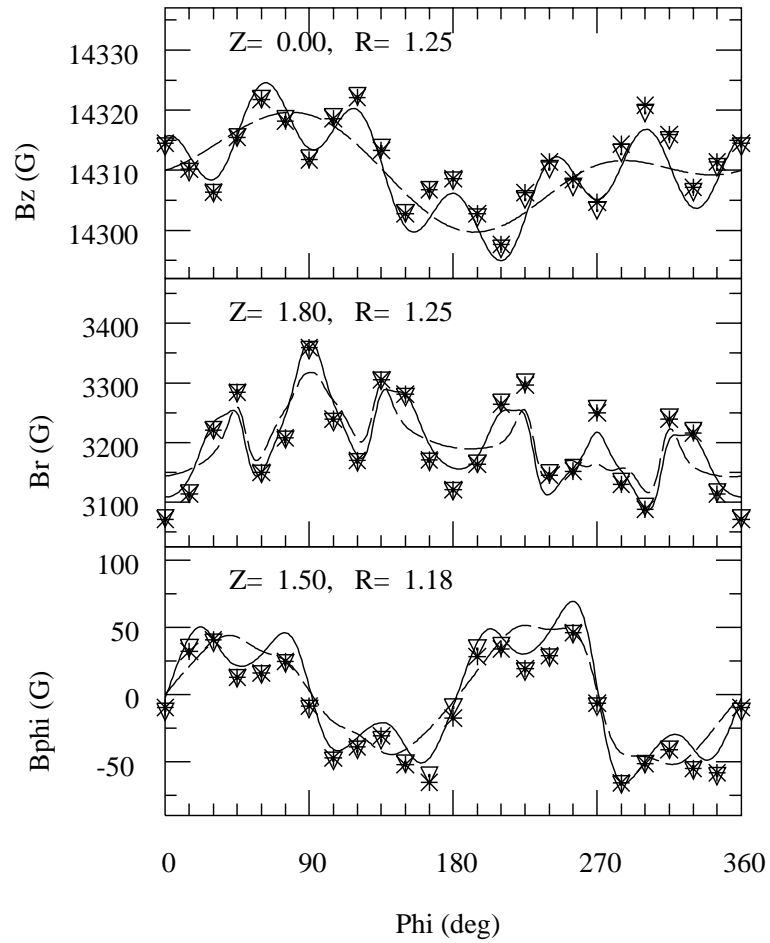


Figure 16. Case c). The field components near the front end plate as a function of ϕ at $R=1.2m$ showing the fit with (solid lines) and without (dashed lines) the $n=6$ Bessel terms. The six peaks in the data every 60 degrees are described by the $n=6$ term in the fit. This six-fold symmetry arises from the hexagonal shape of the barrel iron surrounding the coil.

Fields From Warped Front End Plate

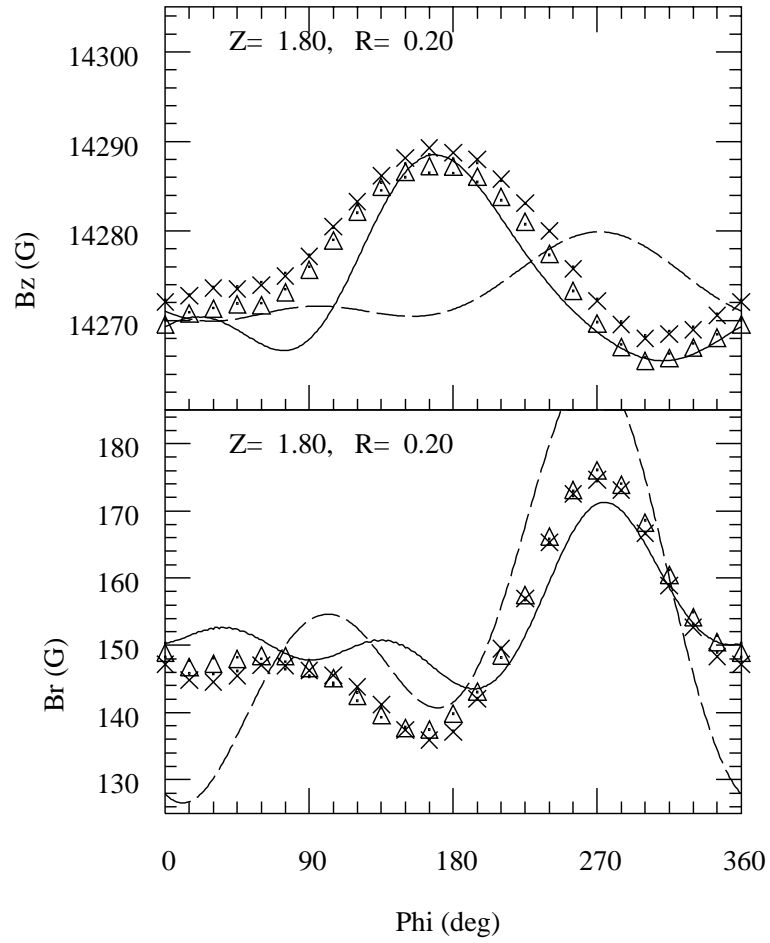


Figure 17. Case d). The Z and R components of the field near the front door, showing the fit with (solid line) and without (dashed line) the annular dipoles at the front end plate. The annular dipoles attempt to describe warped front end plates.

Field Distortions From Cable & Rail Holes

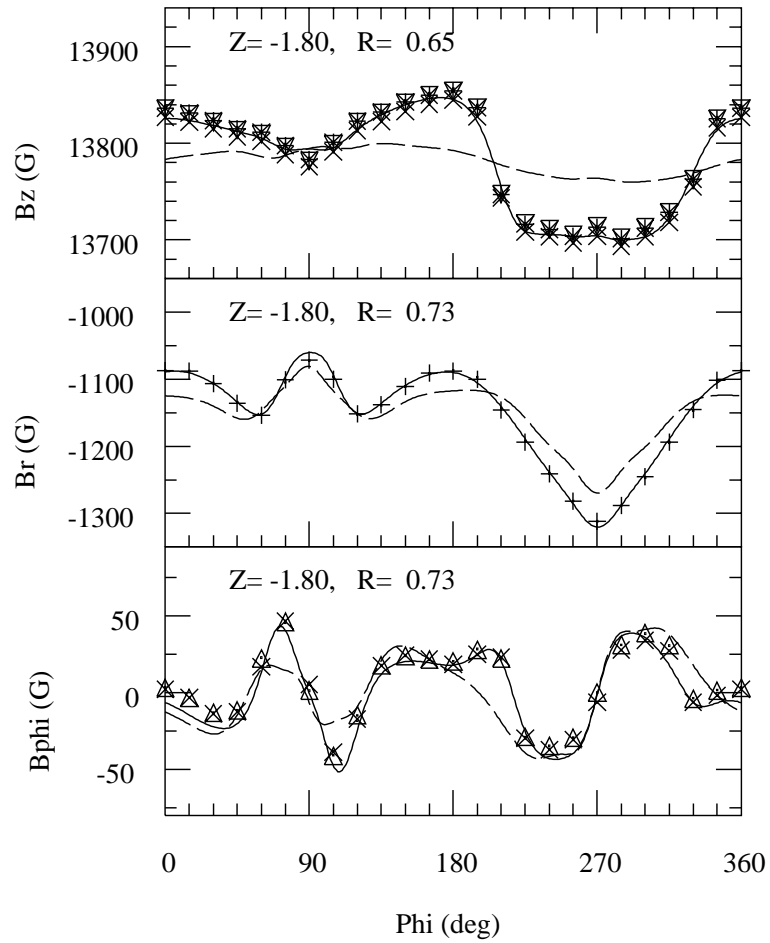


Figure 18. Case e). The field components near the rear door ($Z=-1.8\text{m}$) as a function of ϕ , showing the effects of the cable holes and rail holes in the rear plug. The B_z field has a dip of approximately 120 gauss at $\phi=270$ degrees and $R=0.65\text{m}$.

Field Distortions From Cryostat Flue

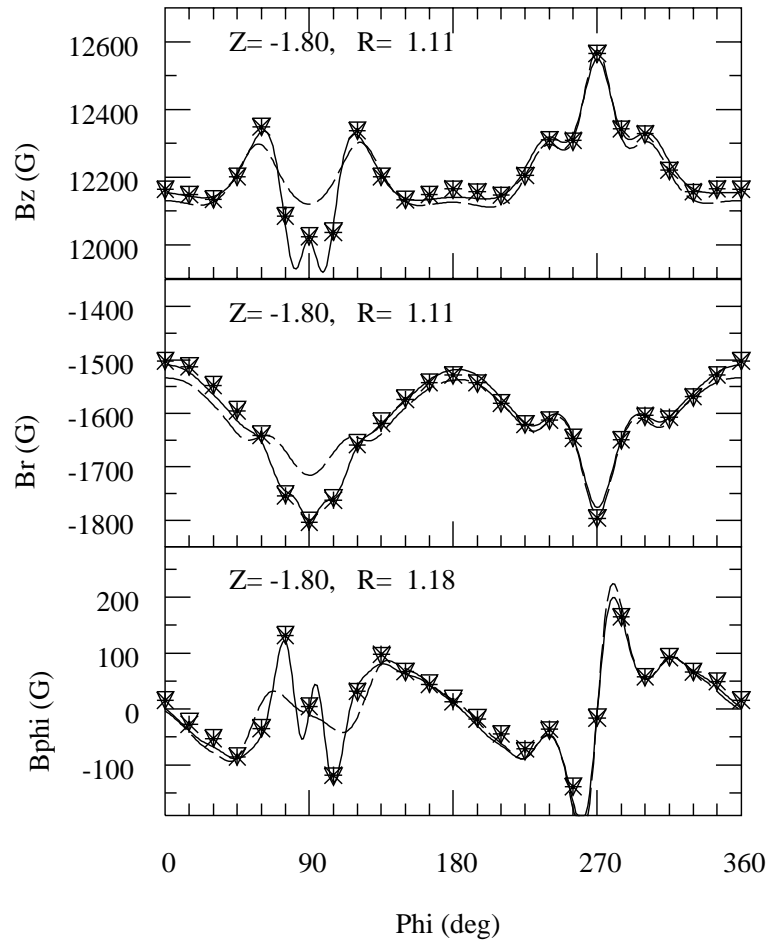


Figure 19. Case f). Field distortions near the rear door ($Z=-1.8\text{m}$) due to the vertical channel at the top of the detector ($\phi=90$ degrees) for the cryogenic utilities.

Field Distortions From IFR Spacers

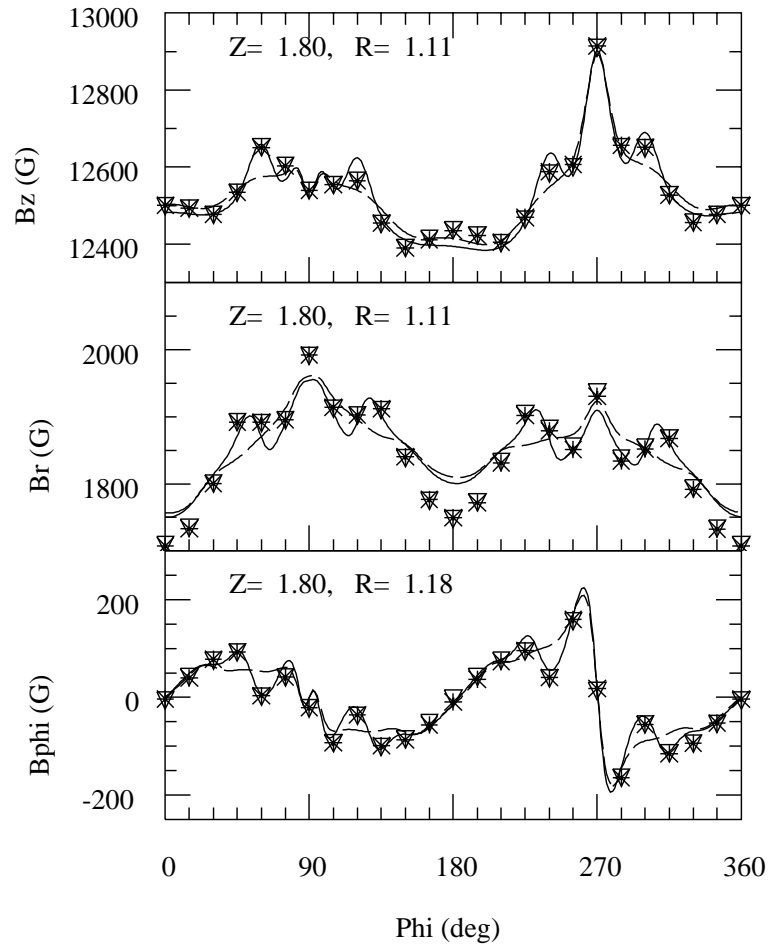


Figure 20. Case g). Field distortions due to the iron spacers in the IFR door plates. The B_z field has peaks of approximately 75 gauss on either side of the upward and downward angles at the locations shown ($Z=1.8m$, $R=1.11m$). The solid curve is the fit to the data, and the dashed line is a fit without including dipole terms for the spacers.

References

1. Bill Dunwoodie, SLAC. The field measurements around the permanent B1 and Q1 magnets have been made, together with a fit to model equations. These results will be given in a future publication.
2. Art Snyder, SLAC. Private communication.
3. SENTRON AG, Two Axes very high accuracy Hall Probe, 2MR-4A/3B-14B25-20. The specification for the B_Z component is 0.01% short term and $<0.1\%$ long term, while the B_R component is 0.1%. Alignment tolerance for both components is $\pm 9\text{mrad}$.
4. SOLVE, A SLAC based least squares fitting program, C. Moore, SLAC, 1965.